Hindawi
Advances in Civil Engineering
Volume 2023, Article ID 4322246, 16 pages
https://doi.org/10.1155/2023/4322246

Research Article

Investigation of Steel I-Beams Strengthened Using CFRP and BFRP Sheets under Torsion

Emine Aydin

Department of Civil Engineering, Faculty of Technology, Sakarya University of Applied Sciences, Sakarya, Turkey

Correspondence should be addressed to Emine Aydin; emineb@subu.edu.tr

Received 21 February 2023; Revised 26 June 2023; Accepted 29 June 2023; Published 18 July 2023

Academic Editor: Krishanu Roy

Torsional demand acting on beams can significantly effect structural behavior and cause high-local stresses. The torsional resistance of beams can be potentially increased by using fiber-reinforced polymer (FRP) sheets. In this study, basalt (BFRP) and carbon (CFRP) fabrics with different layouts are used to strength the steel I-beams, and the enhancement in the torsional strength is investigated experimentally and numerically. First, 12 specimens are reinforced using BFRP and CFRP fabrics bonded to the web of steel I-beams in three different layouts to carry out the experimental study. In total, 14 specimens are tested under torsion including two reference beams. Second, a numerical model is developed to capture the torsional behavior of web-reinforced steel beams. After the numerical model is verified satisfactorily, a parametric study is conducted to evaluate the effect of FRP strengthening on steel beams for flange-only and full reinforcement alternatives. In the experiments, fully web-bonded FRP strengthening configuration achieved 18% and 14% increase in torsional capacities for BFRP and CFRP sheets compared to reference, respectively. In last, it is discovered by the parametric study that the full reinforcement using FRP on the web and flanges can achieve up to 43% increase.

1. Introduction

In structures, beams are subjected to torsion under circumstances such as eccentric loading on the connected cantilever slabs and the continuity of floor beams. Therefore, structural design must satisfy sufficient torsional strength. With respect to torsion, it is seen that experimental and numerical studies have been made for different structural elements [1–5]. Jeng et al. [6] proposed cracking-torque formulas for hollow prestressed concrete beams based on experimental and theoretical results under torsion. Zhou et al. [7] significantly improved the torsional behavior of ultrahigh performance of concrete beams with steel fibers that increased the cracking torque by 79% and the maximum torque by 159%. Furthermore, Kim et al. [8] carried out experimental studies on reinforced concrete members, showing that pure torsional behavior is dependent on cross-sectional properties and the amount of torsional reinforcement. Later, Xin et al. [9] declared that the torsional ductility of channel steel reinforced concrete beams is higher than that of reinforced concrete beams. In addition, Ren et al. [10] investigated the effect of large-diameter stiffened steel tubes used in wind turbines under combined compression–bendingtorsion loads with experimental and the finite element method (FEM). Wan et al. [11] tested the behavior of cold-formed steel beams using C and Z sections under bending and torsional loads. Moreover, Li et al. [12] carried out studies on the nonuniform torsion of thin-walled single or multicell box beams to discover the effects of both bending and shear deformations with FEM. Maali has developed a numerical method that predicts the torsional behavior of steel beams with a sinusoidal web [13]. Last, Wang et al. [14] studied composite box girders with corrugated steel webs to propose an analytical solution for the bending-torsion behavior.

To provide sufficient torsional strength, various strengthening methods are applied to the steel structures. The traditional method of strengthening steel elements involves adding steel plates to existing members by welding or using bolts. The main drawbacks of these methods are an increase in self-weight of the members, stress concentrations in drilled holes and welds, a potential decrease in strength due to the effects of corrosion, and a reduced adaptability of the steel plates, creating complex problems [15]. However, fiber-reinforced polymer (FRP) materials can also be used for the reinforcement of structural steel elements, due to their advantages in terms of

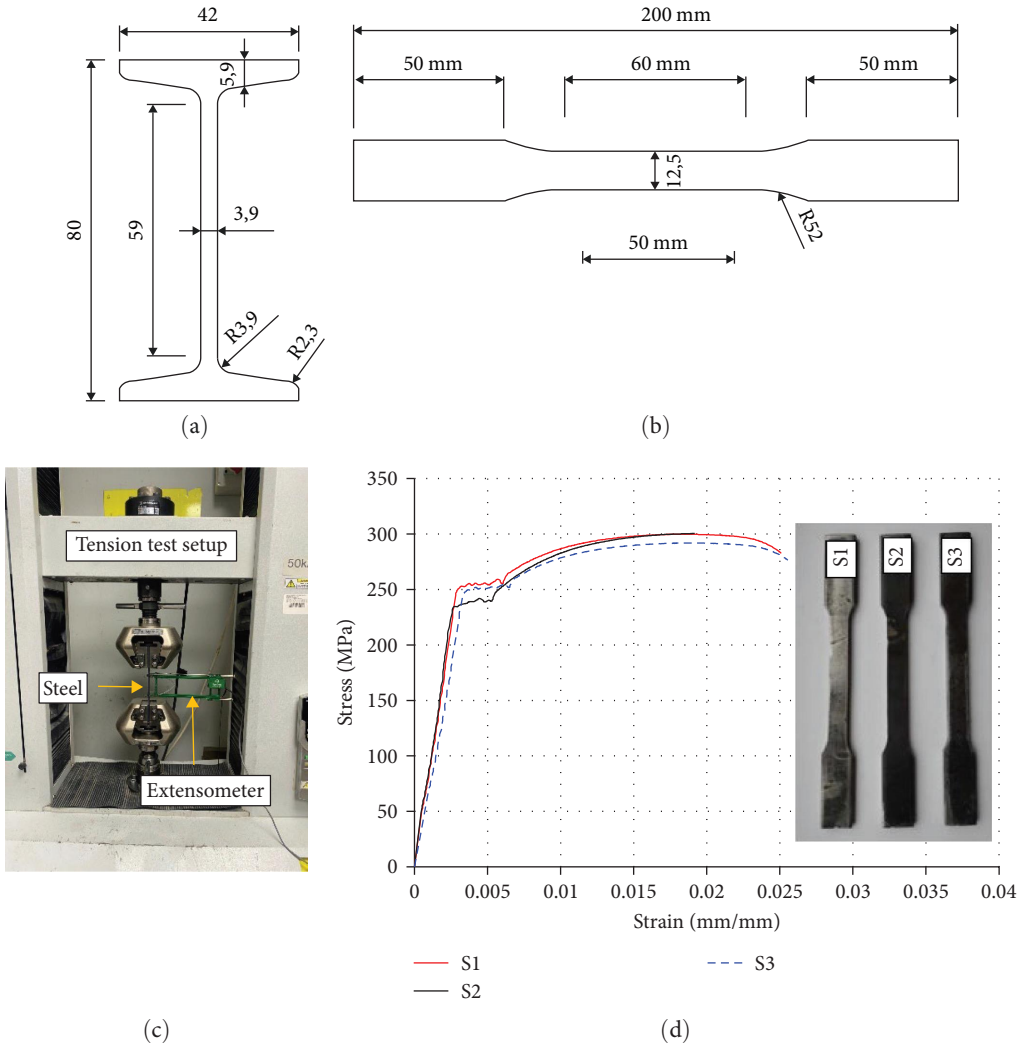

Figure 1: (a) Steel I-beam section for torsion tests, (b) coupon test specimen for tension tests, (c) tension test setup, and (d) tensile stress–strain relationship.

mechanical properties (such as, fatigue and corrosion resistance) [16, 17]. In addition to these, it has been presented in experimental and numerical studies that the mechanical properties of web opening, prefabricated, and hybrid beams can be improved by applying FRPs in different types and layers using FRPs [18–27]. For instance, Kaman et al. [28] applied the neural network to predict the torsional performance of steel beams strengthened by bonding different types of FRPs, emphasizing the reduction of required experimental work with this method. Furthermore, experimental and parametric studies have shown that a permanent repair can be achieved by bonding GFRP plates to steel elements [29, 30]. Ghafoori and Motavalli [31] investigated the elastic behavior of steel beams reinforced with FRP reinforcement under torsion, resulting in a significant increase in the stiffness of the composite beam. In addition, Jariwala et al. [32] experimentally investigated the impact of GFRP reinforcements with different combinations, and the maximum torsional capacity of steel beams increased up to 117%. In contrast, Hadhoo et al. [33] conducted torsion tests on concrete beams reinforced with GFRP spiral rebars at different angles, and new equations are recommended for the design. Moreover, axial pressure and torsion tests were carried out on concrete-filled CFRP-steel tubes where the carbon FRP layer confines the steel tube externally, providing additional corrosion resistance. The experimental results showed that the torsion performance is high, however, this performance will vary depending on the thickness of the CFRP layer and the geometric properties of the steel tube [34, 35]. As can be seen from the studies in the literature, studies examining the torsional behavior of steel beams are very limited. In addition, there is no study examining the torsional behavior of steel beams reinforced using different combinations and different types of FRP. For this reason, this gap in the literature formed the motivation of the study.

For this purpose, this study presents the effect of FRP reinforcements on the torsional behavior of steel I-beams using BFRP and CFRP sheets and different strengthening layouts which have not been adequately investigated in the literature. Hence, both experimental and parametric investigations on their torsional behavior are conducted to evaluate

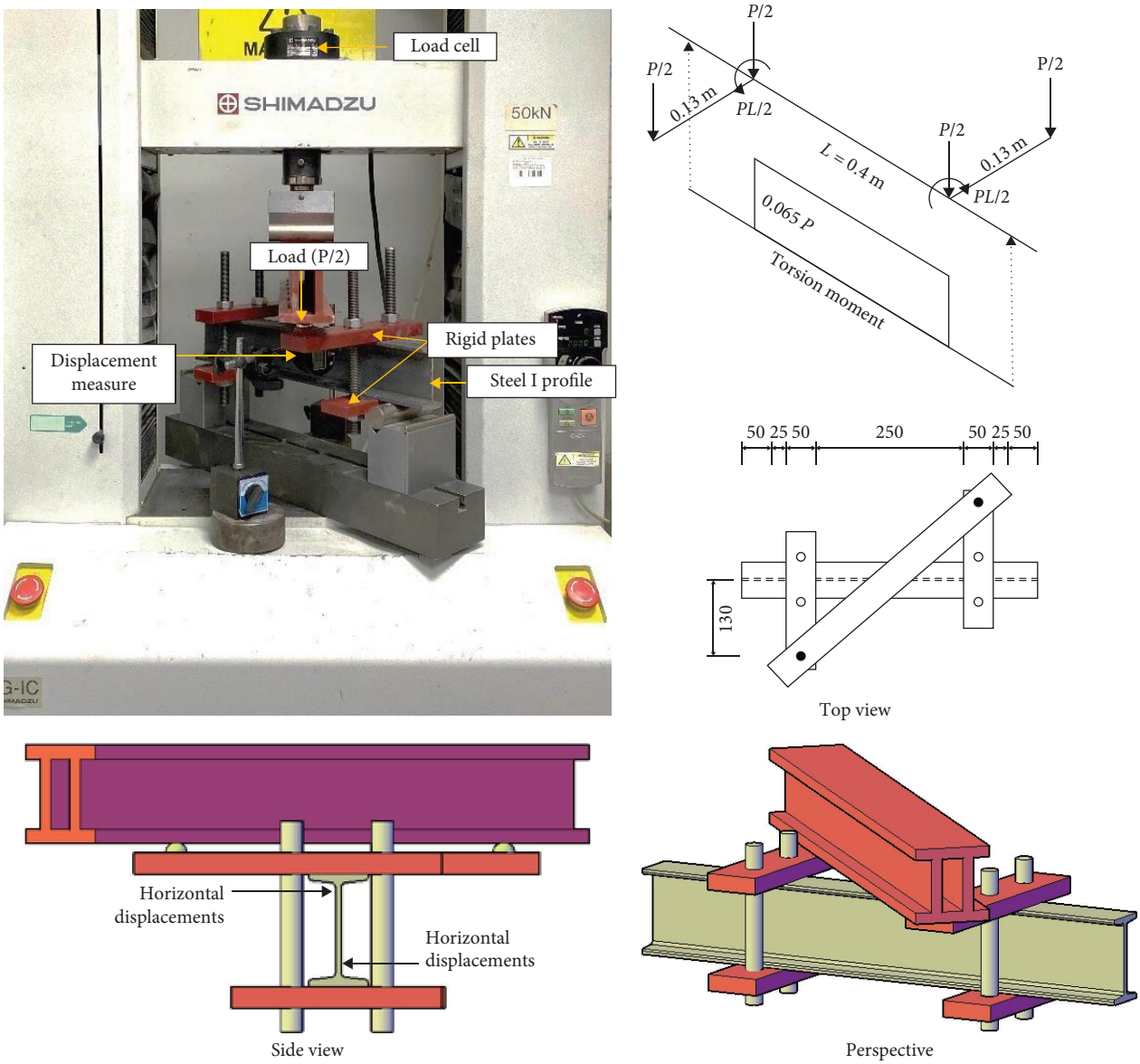

Figure 2: The test setup of steel beams subjected to torsion (units: mm).

the impact of FRP reinforcement built in various fabric combinations and bonded on the surfaces of the web and flanges of steel beams. Experimental tests of reference and reinforced specimens are reported in detail. Then, numerical models are generated using the finite element method and the experimental results are compared with the numerical simulations for the verification. Furthermore, the impact of FRP reinforcement on flanges of steel beams is investigated by a parametric study to assess performances of different strength techniques under torsion.

2. Experimental Study

A series of experimental tests are planned to examine the effect of FRP strengthening by bonding basalt and carbon types of fabric sheets with different layouts applied to the web of steel I-beams under torsion. The test setup is arranged to create torsional demand on steel beams. Except for two reference beam specimens, there different layouts for strengthening purposes were prepared with basalt and carbon FRP sheets to compare the effectiveness of strengthening. Details of FRP layouts are described in the following section. In addition to the reference specimens, two reinforced beam specimens are produced for each strengthening configuration. In total, 14 beam specimens are tested. After the torsion tests, the average values are presented in the results, for clarity.

2.1. Material Properties. In the experimental study, I section profile which is frequently used in steel structures, was chosen and steel beam profile of IPN80 is chosen with S235 material class with the width and thickness of flanges are 42 and 5.9 mm, and the height and thickness of the web

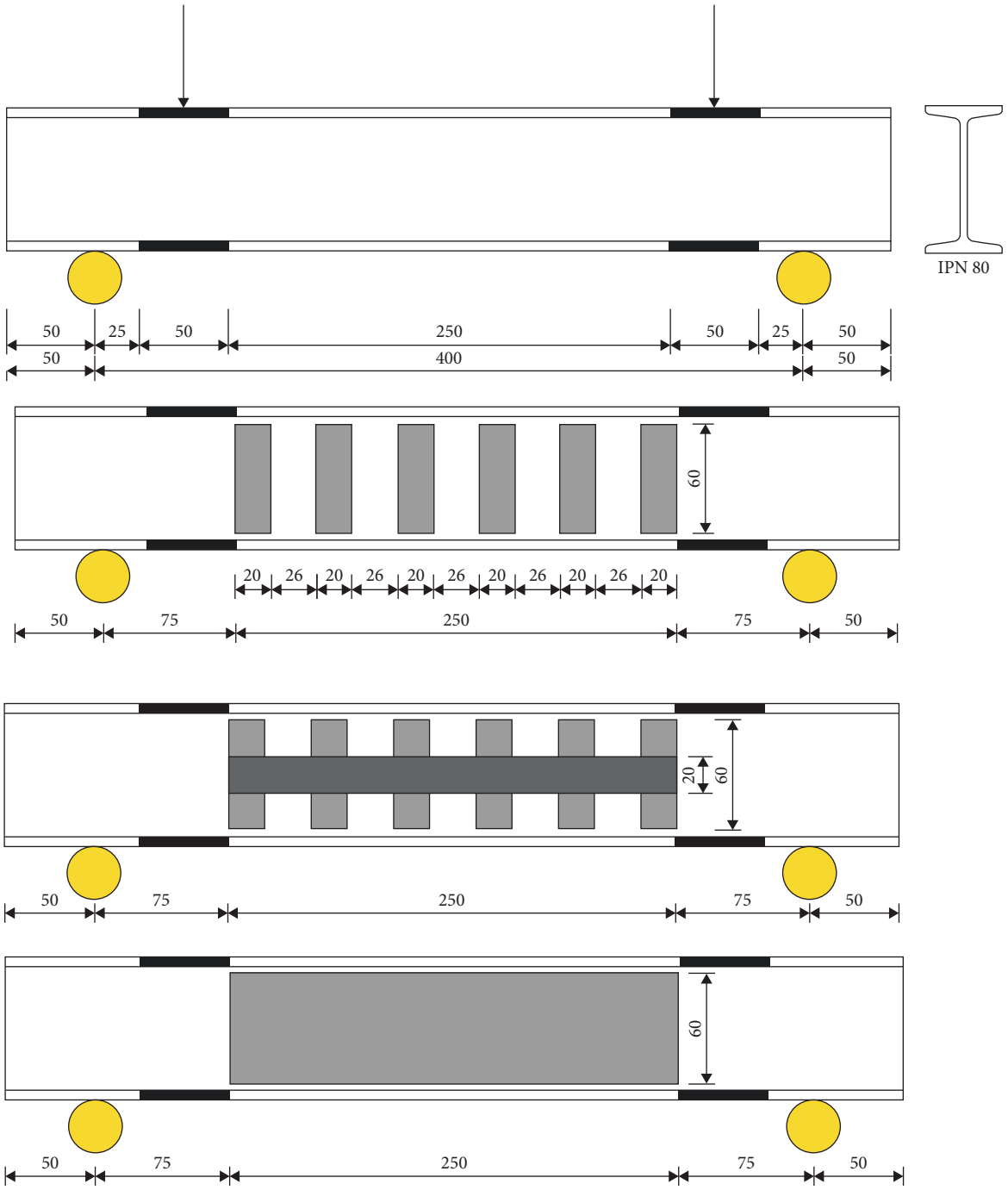

Figure 3: BFRP and CFRP strength schemes for steel beams (units: mm).

are 59 and 3.9 mm, respectively (Figure 1(a)). In order to determine the characteristic properties of steel material, coupon tests are performed on three samples using a tension test setup in accordance with the ASTM A370-10 2010 standard as shown in Figures 1(b) and 1(c) [36]. Next, the tensile stress–strain relationships are presented in Figure 1(d) by using axial deformations and tension loads taken from the extensometer and the machine, respectively.

2.2. Test Setup. For creating torsion demand on the specimens, a testing machine with a capacity of 50 kN is used and the loading speed is automatically given as 2 mm/min. The recording device saves 20 data per second and the data is transferred to the computer. To determine the torsional angle in steel beams, horizontal displacements are measured using linear variable differential transformers (LVDTs) connected to the lower and upper flanges of steel beams.

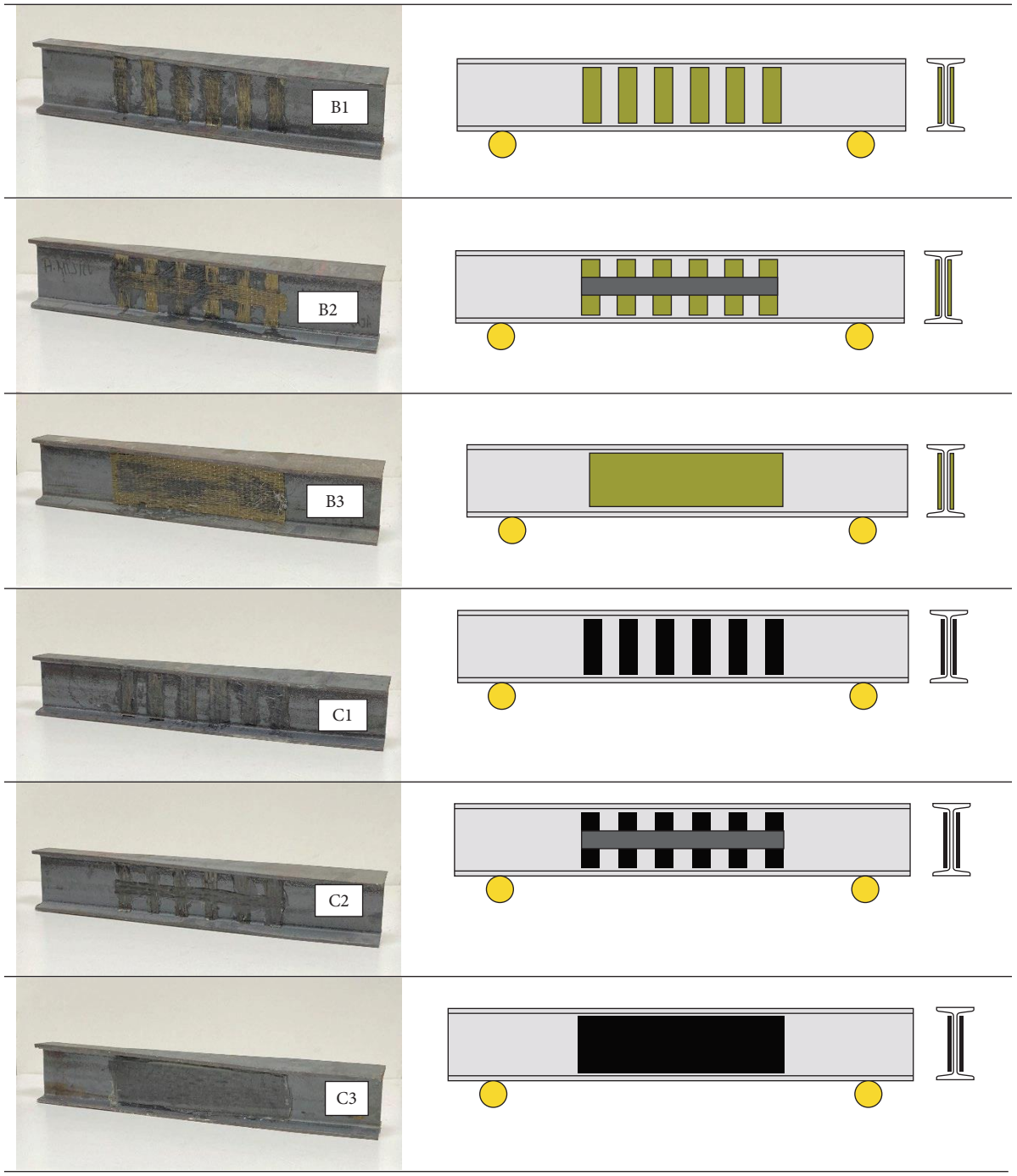

Figure 4: FRP strengthened steel I-beams.

As shown in Figure 2, the load is applied to a rigid plate placed diagonally with respect to the specimen to transfer the load from the rigid plate to the beam for the test setup. With the help of steel shots placed in the small cavities of load transmission element, the applied point load remained constant throughout the experiment without changing its location.

2.3. Preparation of Specimens. Before the experiments, steel I-shaped profiles with an IPN80 section are ordered with a total length of 500 mm spanning 400 mm between supports. The surfaces of the steel elements are cleaned of dirt, oil and rust with a brush. For FRP strengthening, basalt and carbon fabrics are adhered to the web of steel beams in different orientations and at intervals shown in Figure 3. Unidirectional FRPs were applied parallel to the beam length (0^0). Its mechanical properties are CFRP's density 1.79 g/cm^3, tensile strength 3,900 MPa, elastic modulus 230 GPa, and thickness 0.17 mm. BFRP has tensile strength 3,115 MPa, elastic modulus 89 GPa, thickness 0.14 mm, and specific gravity 2.8 g/cm^3. Considering these properties, the ratios of the flange thickness of the steel

Figure 5: The experiment of reference beams under torsion.

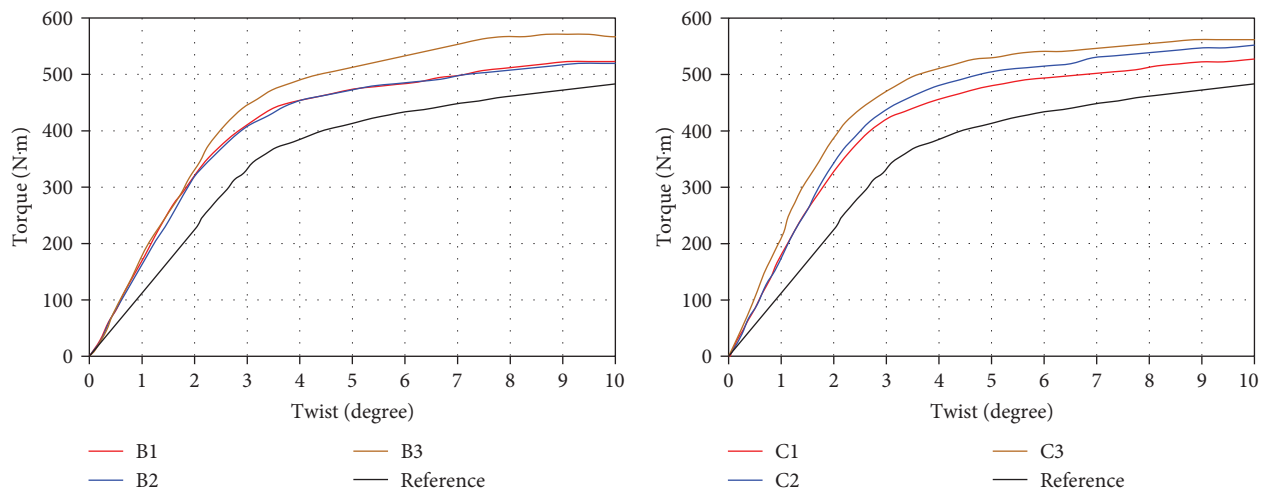

Figure 6: The torque–twist relationship of specimens.

profile to FRP are, respectively 42.14 in BFRP and 34.71 in CFRP. The ratio of steel body thickness to FRP is 27.86 in BFRP and 22.94 in CFRP, respectively.

The first and second strength schemes are represented by two fabric layouts that are configured as intermittent using vertical and vertical + horizontal, respectively. In addition, a third strength scheme is fully bonded to the whole surface of the web to generate an uninterrupted layout, where the strong direction of the fabrics are chosen parallel to the beam section. In total, 14 steel beams are prepared for the experimental study, consisting of two reference, six carbon-reinforced, and six basalt-reinforced specimens. Before the bonding of FRP sheets, the epoxy mixture is prepared as stated by the manufacturer, and a homogeneous distribution of epoxy is ensured by a pressing process in the laboratory. Then, the specimens are left to dry in the ambient climate.

For the notification, steel beams strengthened using basalt FRP sheets are named with the letter "B", and those using carbon FRP sheets are named with the letter "C." For different strength schemes at intervals, "1" describes the vertical placement of fabrics on the web and "2" is for the vertical and horizontal placement of fabrics on the web. However, "3" reprensets a fully bonded layout. The notifications and the beam specimens are shown in Figure 4.

2.4. Experimental Results. First, the reference beam experiments are carried out using IPN80 steel sections without any FRP application in the test setup. The photos before and after the experiments are given in Figure 5. Afterward, other tests are executed, and torque–twist relationships are obtained as shown in Figure 6. After the experiment, it was observed that the adhesive was separated from the steel surface and no damage occurred to the FRPs.

To obtain torquetwist relationships, loads are taken from the testing machine and the torque value is calculated by multiplying the applied point load with the distance between the load and the beam specimen. The twist is measured from the lateral displacements obtained via transducers from the

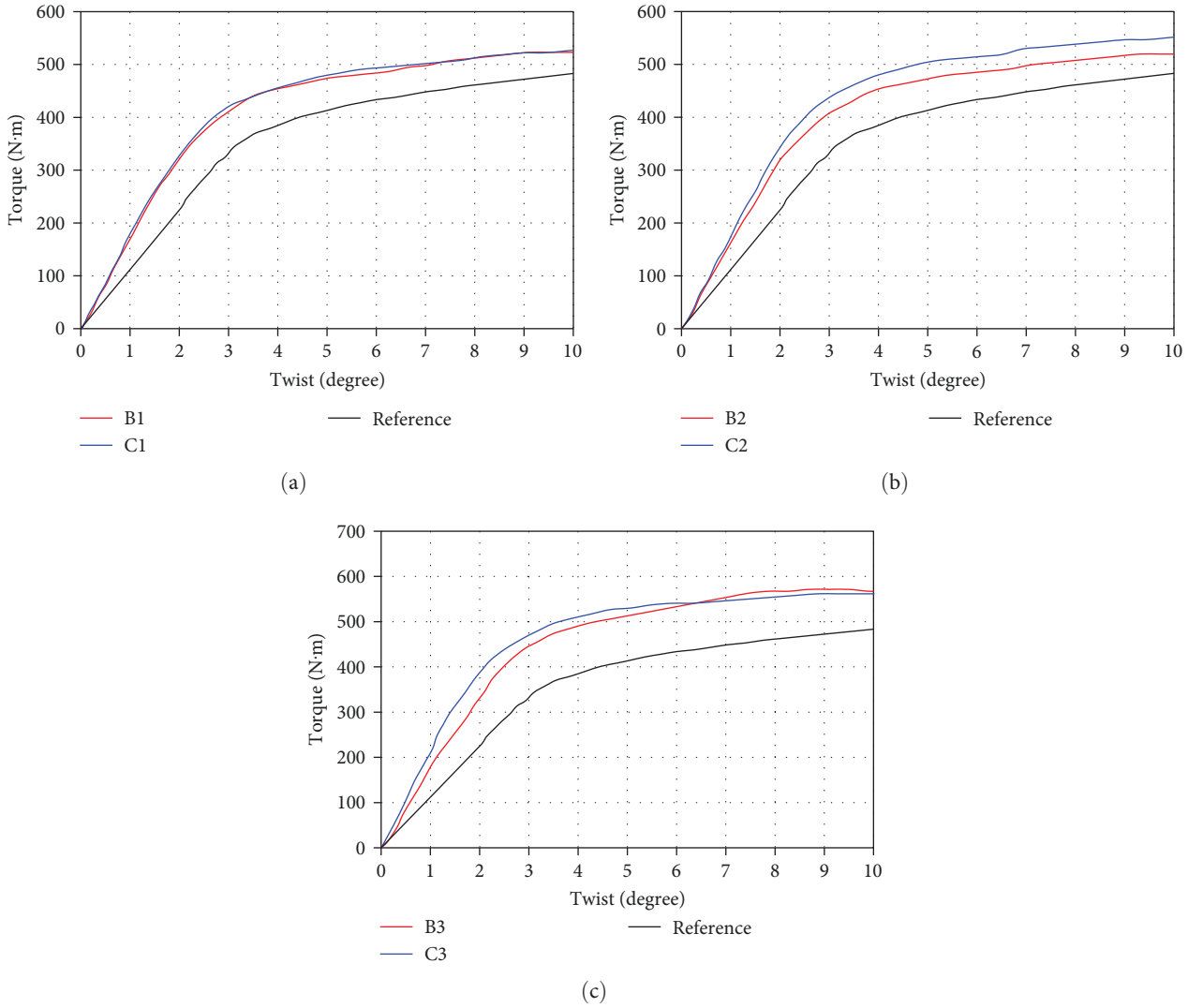

Figure 7: The effect of FRP type on reinforced specimens.

lower and upper points of the beam's flanges of IPN80, as shown in Figure 2.

As shown in Figure 6, the mean result of reference beam specimens has reached a peak torsion of 485.35 N·m. However, the means of the peak torsion capacities (N·m) are improved for the reinforced specimens: B1 = 522.97, B2 = 519.46, B3 = 571.23, C1 = 515.29, C2 = 540.01, and C3 = 554.65. Hence, the highest torsion capacities are found in BFRP and CFRP fabrics with fully bonded web applications named B3 and C3, respectively.

After examining the torsion corresponding to the angle of 2° in the elastic region, capacities (N·m) are obtained as follows: reference = 227.39, B1 = 324.32, B2 = 335.75, B3 = 345.21, C1 = 338.82, C2 = 367.06, and C3 = 394.19. Next, the angles corresponding to the torsion of 314 N·m in the elastic region are evaluated: reference = 2.76°, B1 = 2.03°, B2 = 1.96°, B3 = 1.90°, C1 = 1.92°, C2 = 1.80°, and C3 = 1.55°. Comparing the torsional stiffnesses of the refence beam with the reinforced beam specimens, torsional

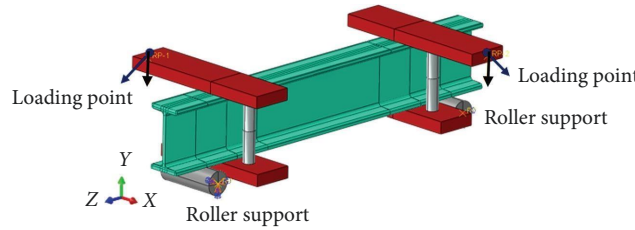

Figure 8: Finite element model with boundary conditions.

stiffnesses are increased by 45%, 45%, 50%, 50%, 57%, and 87% for B1, B2, B3, C1, C2, and C3, respectively.

The effect of the FRP types and the effectiveness of the strength schemes using FRP sheets bonded with different arrangements to the web of beam specimens are shown in Figure 7. Consequently, the torsion capacities are similar in the case of FRP sheets that are vertically bonded at intervals (Figure 7(a)) and fully bonded (Figure 7(c)). However, there is a 3.8% difference between basalt and carbon reinforced

Table 1: The mechanical properties of steel, BFRP, and CFRP sheets.

Material	Yield stress (MPa)	Tensile strength (MPa)	Elastic modulus (GPa)	Rupture ratio (%)
Steel	240	282	200	38
BFRP	–	3,900	230	1.5
CFRP	–	3,115	89	3.5

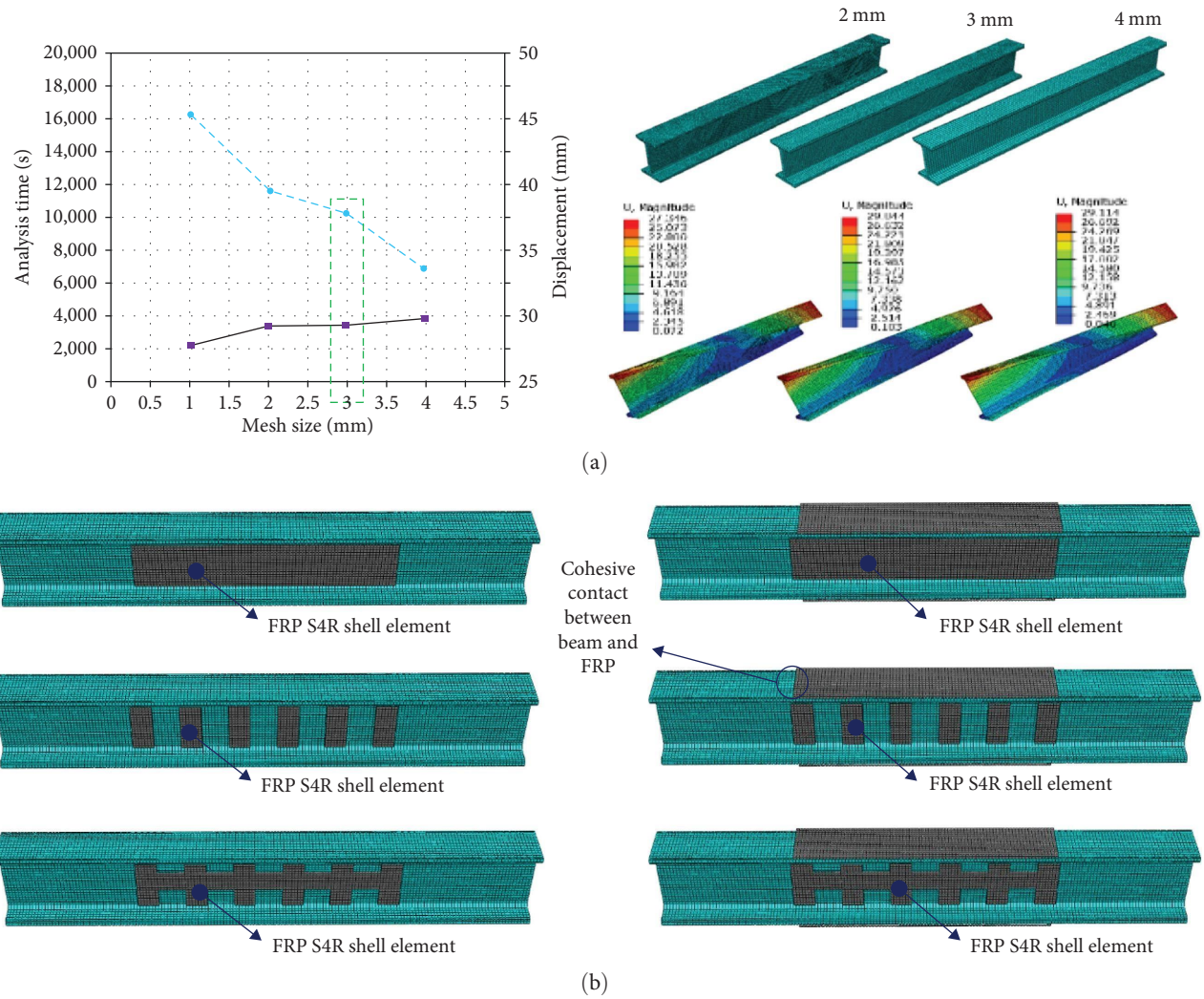

Figure 9: (a) Mesh sensivity and (b) meshing sizes in the finite element method.

specimens using vertically and horizontally placed fabric on the web (Figure 7(b)). Thus, it could be interpreted that a fully web-bonded FRP strength scheme (Figure 7(c)) provides better performance compared to vertical and horizontal bonding with intervals (Figure 7(b)) due to the prevention of crack propagation in the adhesive.

The improvements, however, are more noticeable in the elastic region. For instance, the capacities corresponding to the same angle as the reference specimen are increased by 42.63%, 47.65%, and 51.81%, and 49.01%, 61.42%, and 73.35% for basalt and carbon reinforced specimens, respectively. According to the test results of the reference and reinforced specimens, basalt and carbon fibers applied to a steel surface provide an increase in torsional capacity ranging from 42%–73%. Similarly, the angles corresponding to the same torsional demand are evaluated in the elastic region. In consequence, the angles are decreased by 26.50%, 28.79%, and 31.15% for basalt fiber sheets (B1, B2, and B3) and by 30.28%, 34.59%, and 43.65% for carbon fiber sheets (C1, C2, and C3), respectively, compared to the reference specimen.

The torsional angle of the reference beams in the elastic region is also verified by the formula given in Equation 1 [37]. Where θ is the torsion angle, T is the torsion, L is the specimen length, c_1, a, b are numbers obtained from the cross-sectional properties of beam specimens, and G is the shear modulus of the steel material. From Equation 2, the torsional

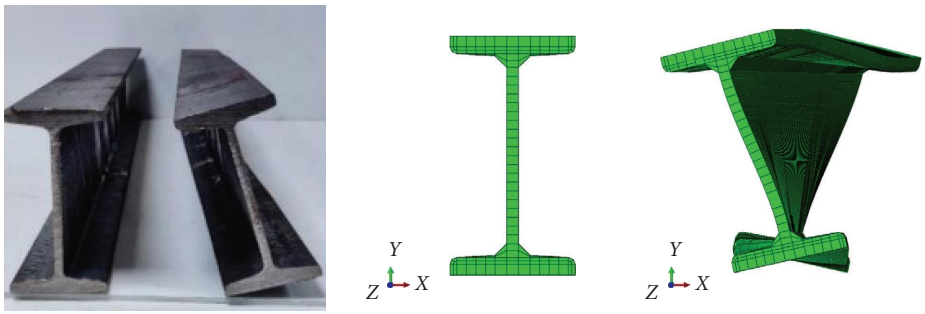

Figure 10: Experiment and numerical model.

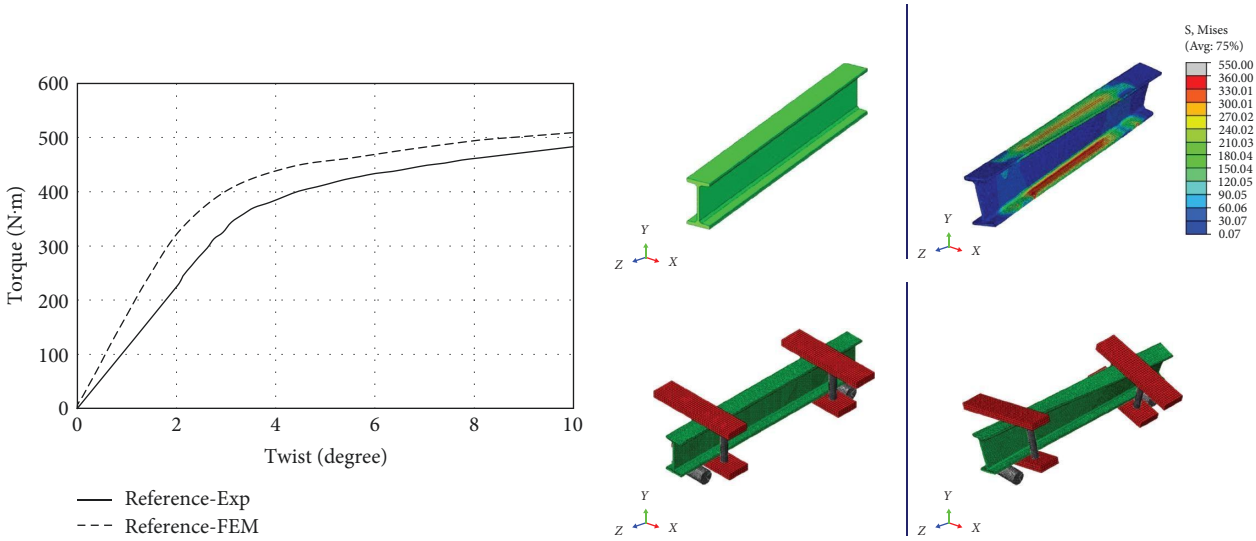

Figure 11: Validation study of the reference models.

stiffnesses of all test combinations were calculated [37]. Here k is the torsional stiffness and J is the polar moment of inertia.

$$\theta = \frac{T \cdot L}{c_1 a b^3 G}, \tag{1}$$

$$k = \mathrm{GJ}/L. \tag{2}$$

The polar moments of inertia were calculated from the obtained torsional stiffnesses. According to the reference polar moment of inertia, B1 49%, B2 41%, B3 50%, and C1 44%, C2 52%, C3 80% increases were obtained.

3. Finite Element Modeling

In the finite element method, the objective is to create a refined numerical model capturing the torsional behavior of steel beams taking into account nonlinear material properties and ductile damage patterns by using ABAQUS software [38]. The studies in the literature present that the initial geometric imperfections and residual stresses are used in some finite element models [39–43]. However, the aim of the study is to investigate the effect of FRP on the torsion of steel I-beams. Therefore, the initial geometric imperfections and residual stresses are neglected, as the primary variable is the properties of FRP reinforcement.

First, three-dimensional continuous finite element models of specimens are generated with the boundary conditions. As depicted in Figure 8, IPN80 sections are used for steel beams and reinforced with various FRP schemes. Subsequently, the numerical models are developed in order to examine the effects of basalt and carbon-FRP sheets utilizing various FRP strengthening configurations in a parametric study.

For the steel material, the Poisson ratio and Young's modulus are set at 0.3 and 200 GPa, respectively. Using the Hashin damage criterion provided by the ABAQUS software and assuming that the linear elastic behavour of FRP composite sheets, numerical models are assessed along with the damage identification. The mechanical characteristics of steel materials, BFRP, and CFRP sheets are listed in Table 1.

For steel sections, eight-node solid elements with reduced integration technique (C3D8R) and four-node S4R shell elements were employed for steel and FRP sections, respectively. In the case of contact surfaces between the steel beam and FRP materials, as depicted in Figure 9, the cohesive behavior properties were considered. Numerical analyses are performed using mesh sizes of 2, 3, and 4 mm as seen in Figure 9(a). For the mesh sensivity, 3 mm is found adequate. Therefore,

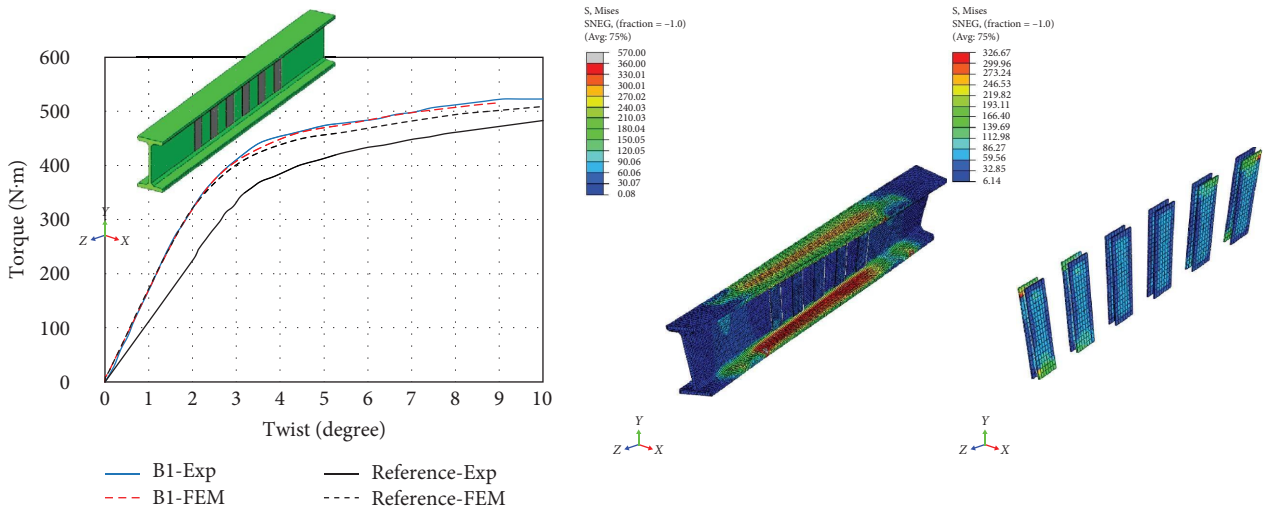

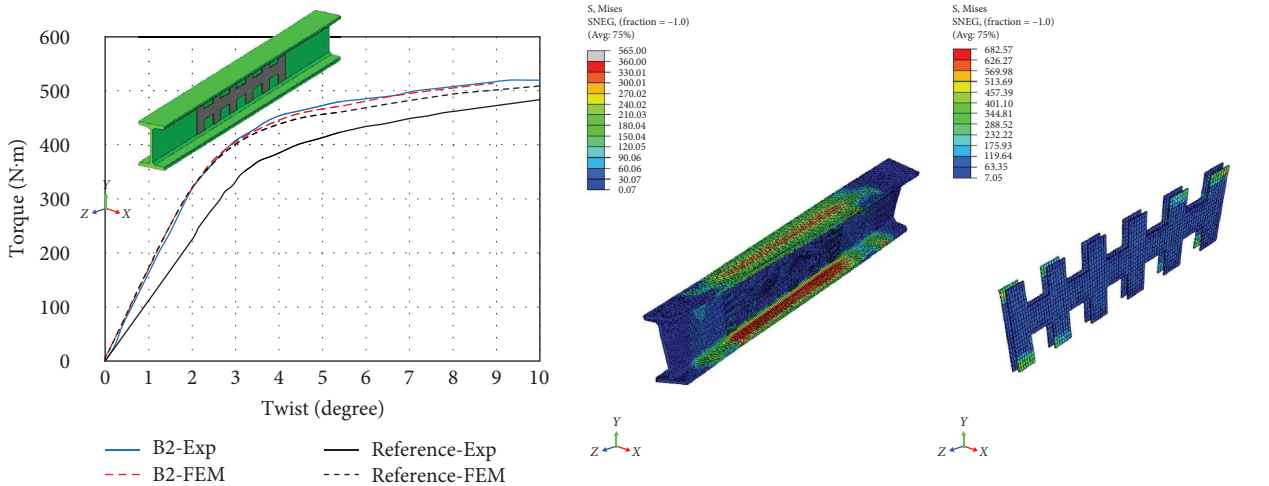

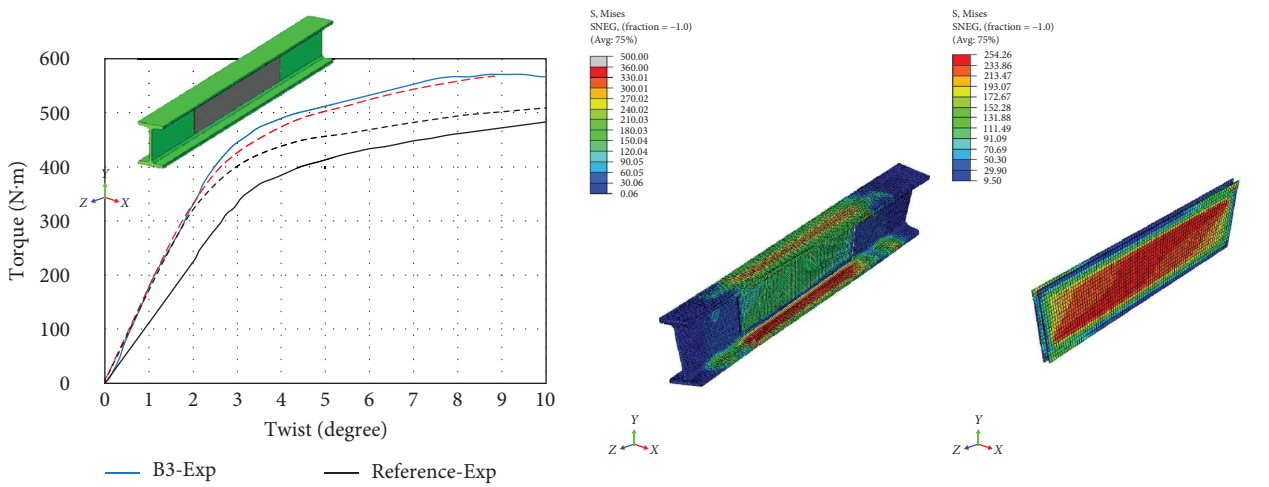

Figure 12: Continued.

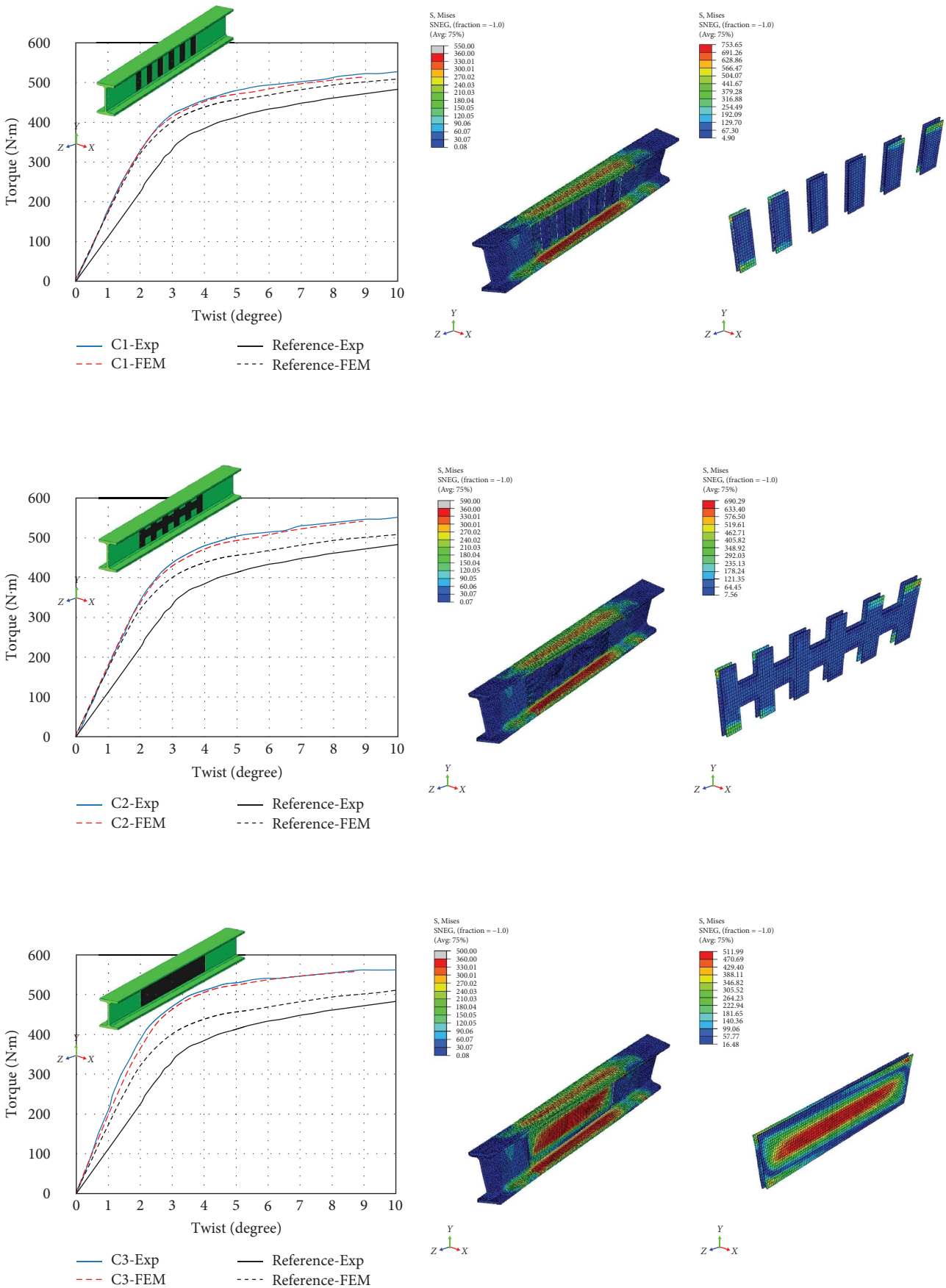

Figure 12: Validation study of the reinforced models.

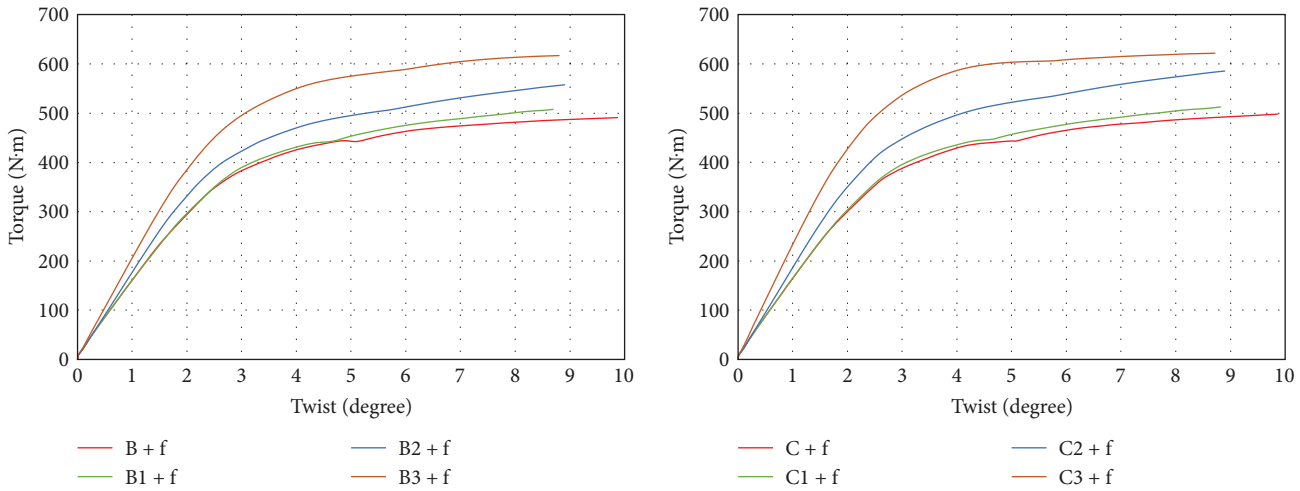

Figure 13: Numerical models of the parametric study for flange-reinforced specimens.

the mesh size for the steel beams and FRP sections is set at 3 mm. Figure 8 depicts the configuration of numerical models with boundary conditions and torsion loading in accordance with the test setup.

Next, a finite element model is generated and validated using the experimental data of reference beams as shown in Figures 10 and 11, respectively. After the verification of reference specimens, CFRP and BFRP reinforced specimens are studied for validation and the comparison of experimental and numerical results can be seen in Figure 12.

4. Parametric Study

After numerical models are verified by laboratory results, a parametric study is executed to address the potential improvement of torsional capacities using FRP sheets on the flanges of steel beams in addition to experimental tests on web reinforcement. Hence, additional specimens are generated numerically using FEM and flange-reinforced specimens are called "B + f" for BFRP and "C + f" for CFRP sheets, respectively. As a result, the numerical models of flange-reinforced specimens are presented in Figure 13 according to each FRP type used for strengthening. Moreover, the effects of FRP strengthening for CFRP and BRFP sheeting are investigated, and FEM results are presented in Figure 14.

As shown in Figures 13 and 14, the torsional capacities are similar for basalt or carbon FRP sheets applied to webs and flanges. Next, experimental and numerical results are presented in Figure 15 to compare and observe the potential enhancement using FRP strengthening applied to both webs and flanges of steel beams.

Considering the peak torsion moments acting on the steel beams, additional BFRP strengthening on flange surfaces resulted with an increase of 5%, 27.49%, and 20.08% for B1 + f, B2 + f, and B3 + f compared to web-only reinforced counterparts of B1, B2, and B3, respectively. However, CFRP strengthening is found to be more effective resulting in an increase of 8.41%, 12.86%, and 43.39% for C1 + f, C2 + f, and C3 + f, respectively, when compared to their web-only reinforced counterparts of C1, C2, and C3. Furthermore, experimental and numerical results are compared for web-only and flange-only reinforced specimens, respectively. Consequently, web-only reinforced specimens have greater peak torsion capacities by 16.32% and 11.33% compared to flange-only reinforced specimens for BFRP and CFRP strengthening, respectively.

For the evaluation of the torsion occurring at the same angle in the elastic region, the torsional capacities of "B1"–"B1 + f", "B2"–"B2 + f," "C1"–"C1 + f," and "C2"–"C2 + f" decreased by 10.75%, 2.37%, 12.66%, and 2.14%, respectively, compared for web-reinforced and full-reinforced specimens using FRP sheets at interval. In fully bonded FRP web application, however, the torsion capacities of "B3"–"B3 + f" and "C3"–"C3 + f" increased by 13.37% and 10.50%, respectively. As it is anticipated, the angle value is diversely related to torsion capacity in the elastic region. After the evaluation of the angle values corresponding to the same torsion, the angles of "B1"–"B1 + f," "B2"–"B2 + f," "C1"–"C1 + f," and "C2"–"C2 + f" increased by 11.29%, 0.25%, 17%, and 14.75%, respectively. However, the angles of "B3"–"B3 + f" and "C3"–"C3 + f" decreased by 7.06% and 7.98%, respectively. Last, the stiffnesses of the reinforced specimens are ordered from smallest to largest as follows: "C + f," "B + f," B1 + f," "C1 + f," "B2 + f," "C2 + f," "B3 + f," and "C3 + f".

Considering the torsional capacity occurring at the same angle in the elastic region, the range of capacity change is 2%–11% for BFRP strength and 2%–13% for CFRP strength. However, when the angle value corresponding to the same torsional demand in the elastic region is considered, the range of angle change is observed in between 0.25%–11% and 8%–14% for BFRP and CFRP strength techniques, respectively. In terms of torsional stiffness, CFRP web reinforcement was found to be the least effective. Full CFRF reinforcement applied to the web and flanges resulted in greater torsional stiffness among the FRP strength solutions.

5. Conclusion

In this study, an experimental campaign is carried out first to strength steel I-beams using CFRP and BFRP sheets to

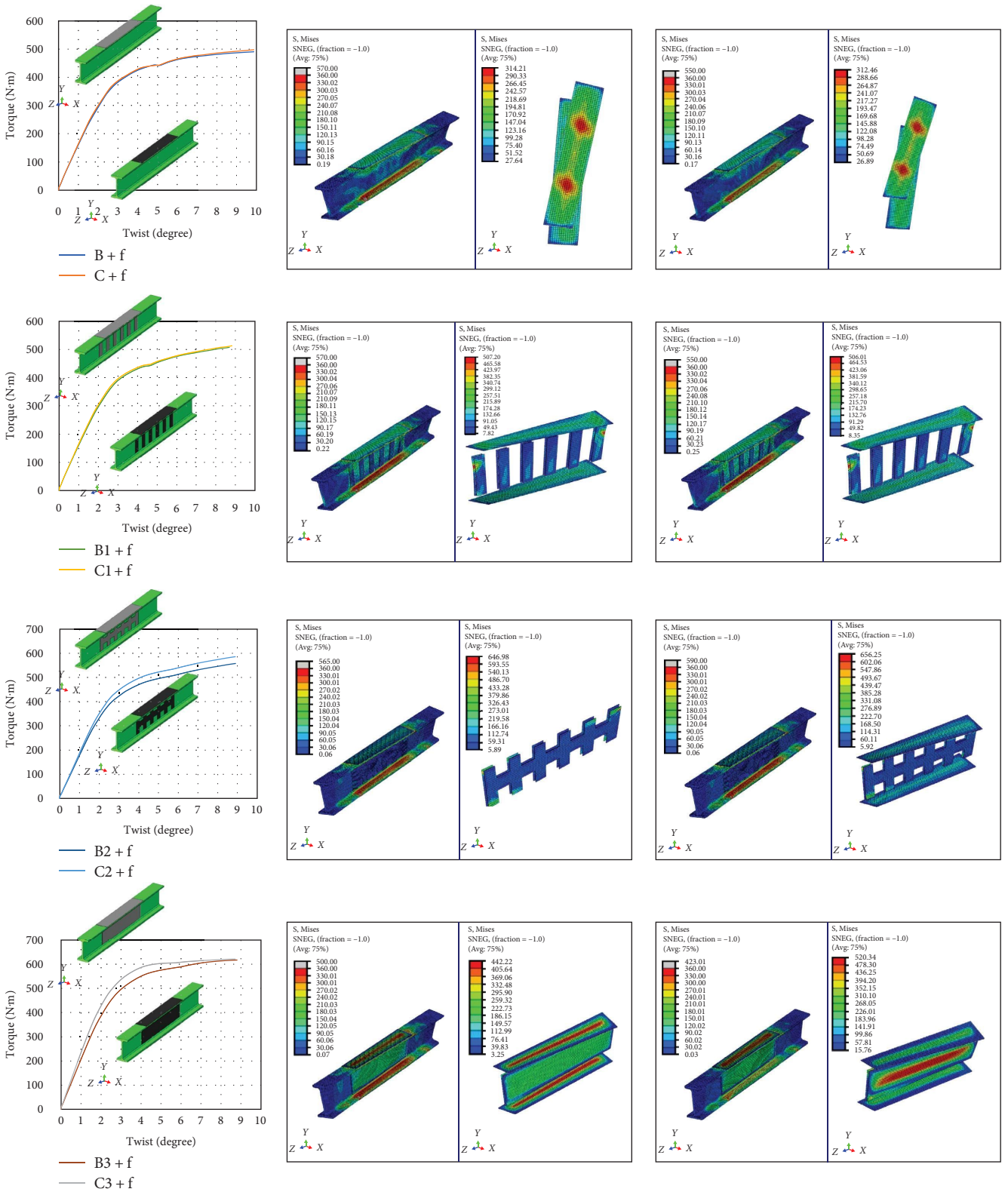

Figure 14: The effect of FRP sheeting for flange-reinforced specimens.

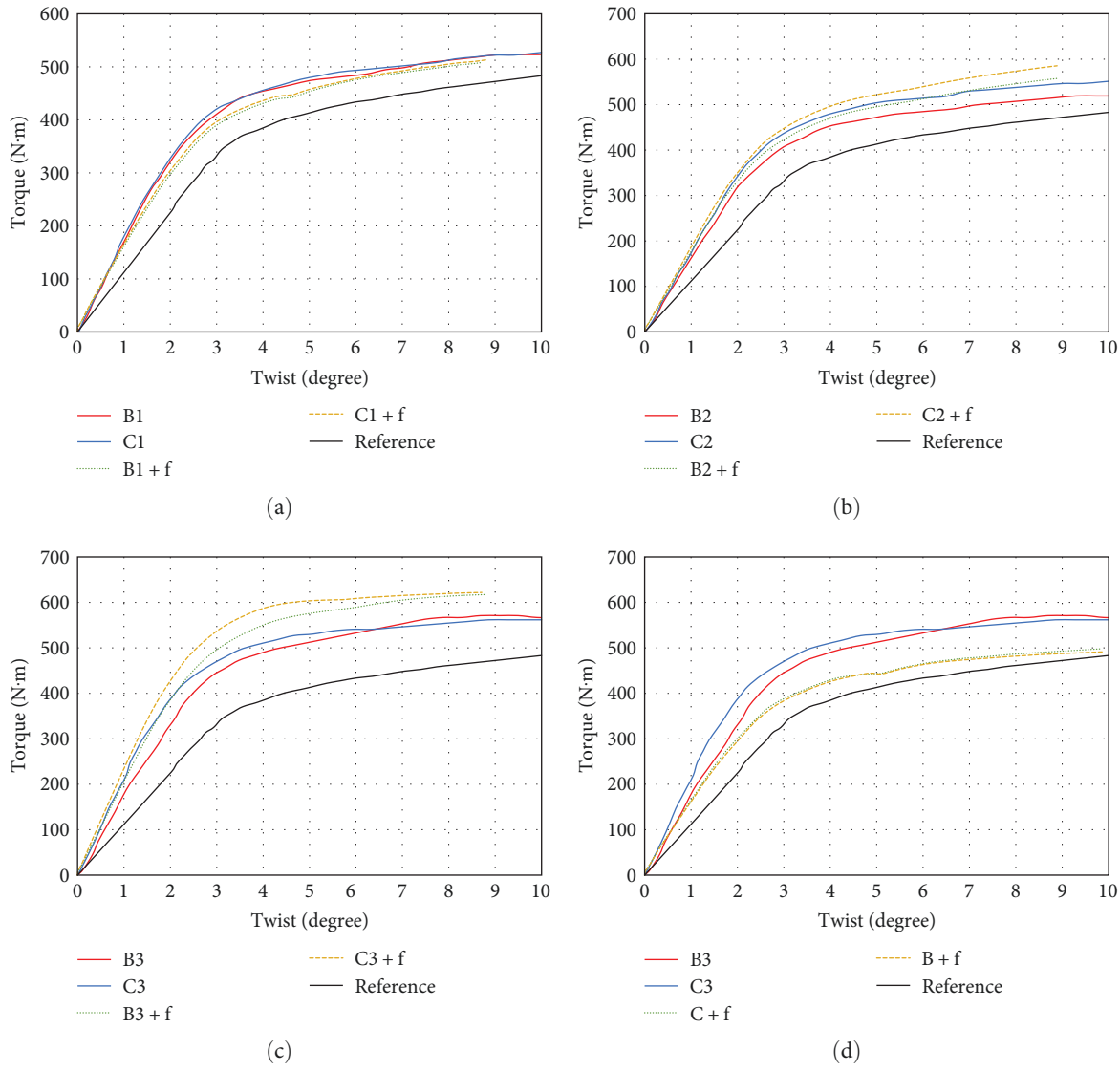

Figure 15: Comparison of the experimantal and numerical results: web-reinforced and flange-reinforced specimens.

invesitigate the potential improvement in the torsional strength and behaivior. Carbon and basalt fabrics are bonded to the web of specimens in three different layouts. In addition, parametric studies are carried out on different FRP sheets applied to the flanges of steel beams using the finite element models that were validated by the experimental test results. Then, the experimental results of web-reinforced steel beams and the numerical results of steel beams strengthened with flange-only, and full reinforcements are compared with reference specimens in terms of fabric types, FRP configurations, peak torsion capacities, and torsional behavior such as, the stiffness in the elastic range. The critical findings of the experimental and parametric studies are summarized below:

(i) In the experiments, the FRP strengthening applied to the web of steel beams increased peak torsional capacities by 7.75%, 7.03%, and 17.70% for basalt fibers (B1, B2, and B3) and by 6.17%, 11.26%, and 14.28% for carbon fibers (C1, C2, and C3) compared to the reference specimen. Furthermore, specimens can be listed according to the lowest to highest torsional stiffnesses: reference, B2, B1, C1, B3, C2, and C3. It should be noted that the peak torsion capacities are higher when carbon fabrics are used and CFRP sheets are bonded fully to the web of reinforced beam specimens.

(ii) After the paremetric study, considering peak torsion on steel I-beams, the web-only and full BFRP strength enhanced the torsional capacities by approximately 5% and 27%, respectively. In addition, CFRP sheets increased the torsional capacities by about 8% and 43% for web-only and full applications, respectively. Finally, it can be concluded that the web reinforcement using FRP sheets resists higher torsion forces compared to flange-only strengthening after comparing the numerical results of flange-only reinforcements and the experimental results of web-only reinforcements.

Data Availability

The data used to support the findings of this study are included within the article.

Conflicts of Interest

The author declares that there is no conflicts of interest.

References

[1] C. Shen, Y. Song, L. Yan, Y. Li, X. Wang, and S. He, "Experimental behavior of the curved continuous twin I-girder composite bridge with a precast concrete slab subjected to bending, shear, and torsion," *Advances in Civil Engineering*, vol. 2020, Article ID 8834773, 16 pages, 2020.

[2] J. Choi and S.-C. Lee, "Sectional analysis procedure for reinforced concrete members subjected to pure torsion," *Advances in Civil Engineering*, vol. 2019, Article ID 6019321, 13 pages, 2019.

[3] N. Askandar and A. Mahmood, "Comparative investigation on torsional behaviour of RC beam strengthened with CFRP fabric wrapping and near-surface mounted (NSM) steel bar," *Advances in Civil Engineering*, vol. 2019, Article ID 9061703, 15 pages, 2019.

[4] J. Xu, B. Diao, Q. Guo, Y. Ye, Y. L. Mo, and T. Zhou, "Parametric study on mixed torsional behavior of U-shaped thin-walled RC girders," *Advances in Civil Engineering*, vol. 2018, Article ID 3497390, 18 pages, 2018.

[5] M. A. El-Mandouh, J. W. Hu, W. S. Shim, F. Abdelazeem, and G. ELsamak, "Torsional improvement of RC beams using various strengthening systems," *Buildings*, vol. 12, no. 11, Article ID 1776, 2022.

[6] C.-H. Jeng, M. Chao, and H.-C. Chuang, "Torsion experiment and cracking-torque formulae of hollow prestressed concrete beams," *Engineering Structures*, vol. 196, Article ID 109325, 2019.

[7] C. Zhou, J. Wang, W. Jia, and Z. Fang, "Torsional behavior of ultra-high performance concrete (UHPC) rectangular beams without steel reinforcement: experimental investigation and theoretical analysis," *Composite Structures*, vol. 299, Article ID 116022, 2022.

[8] M.-J. Kim, H.-G. Kim, Y.-J. Lee, D.-H. Kim, J.-Y. Lee, and K.-H. Kim, "Pure torsional behavior of RC beams in relation to the amount of torsional reinforcement and cross-sectional properties," *Construction and Building Materials*, vol. 260, Article ID 119801, 2020.

[9] Z. Xin, X. Jianyang, R. Rui, and M. Linlin, "Test on pure torsion behavior of channel steel reinforced concrete beams," *Journal of Building Engineering*, vol. 44, Article ID 102967, 2021.

[10] W. Ren, X.-H. Zhou, Z.-L. Fu et al., "Static behavior of large-diameter stiffened steel tubes for wind turbine towers under combined compression-bending-torsion load," *Thin-Walled Structures*, vol. 175, Article ID 109272, 2022.

[11] H.-X. Wan, B. Huang, and M. Mahendran, "Experiments and numerical modelling of cold-formed steel beams under bending and torsion," *Thin-Walled Structures*, vol. 161, Article ID 107424, 2021.

[12] X. Li, S. Wan, K. Shen, and P. Zhou, "Finite beam element with exact shape functions for torsional analysis in thin-walled single- or multi-cell box girders," *Journal of Constructional Steel Research*, vol. 172, Article ID 106189, 2020.

[13] M. Maali, "Experimental and numerical prediction of torsional behavior of steel beam with sinusoidal web," *Iranian Journal of Science and Technology, Transactions of Civil Engineering*, vol. 44, no. S1, pp. 1–10, 2020.

[14] C. Wang, Y. Zhang, X. Zhang, Y. Li, and X. Wei, "Coupled bending-torsion behaviour of single-box multi-cell curved composite box-girders with corrugated-steel-webs," *Journal of Constructional Steel Research*, vol. 196, Article ID 107411, 2022.

[15] A. Bastani, S. Das, and S. Y. Kenno, "Flexural rehabilitation of steel beam with CFRP and BFRP fabrics—a comparative study," *Archives of Civil and Mechanical Engineering*, vol. 19, no. 3, pp. 871–882, 2019.

[16] C. S. Madan, S. Munuswamy, P. S. Joanna, B. G. A. Gurupatham, and K. Roy, "Comparison of the flexural behavior of high-volume fly AshBased concrete slab reinforced with GFRP bars and steel bars," *Journal of Composites Science*, vol. 6, no. 6, Article ID 157, 2022.

[17] C. S. Madan, K. Panchapakesan, P. V. Anil Reddy et al., "Influence on the flexural behaviour of high-volume fly-ash-based concrete slab reinforced with sustainable glass-fibre-reinforced polymer sheets," *Journal of Composites Science*, vol. 6, no. 6, Article ID 169, 2022.

[18] C. Aksoylu, Ş. Yazman, Y. O. Özkılıç, L. Gemi, and M. H. Arslan, "Experimental analysis of reinforced concrete shear deficient beams with circular web openings strengthened by CFRP composite," *Composite Structures*, vol. 249, Article ID 112561, 2020.

[19] Y. O. Özkılıç, C. Aksoylu, Ş. Yazman, L. Gemi, and M. H. Arslan, "Behavior of CFRP-strengthened RC beams with circular web openings in shear zones: numerical study," *Structures*, vol. 41, pp. 1369–1389, 2022.

[20] L. Gemi, C. Aksoylu, Ş. Yazman, Y. O. Özkılıç, and M. H. Arslan, "Experimental investigation of shear capacity and damage analysis of thinned end prefabricated concrete purlins strengthened by CFRP composite," *Composite Structures*, vol. 229, Article ID 111399, 2019.

[21] L. Gemi, E. Madenci, and Y. O. Özkılıç, "Experimental, analytical and numerical investigation of pultruded GFRP composite beams infilled with hybrid FRP reinforced concrete," *Engineering Structures*, vol. 244, Article ID 112790, 2021.

[22] Y. O. Özkılıç, Ş. Yazman, C. Aksoylu, M. H. Arslan, and L. Gemi, "Numerical investigation of the parameters influencing the behavior of dapped end prefabricated concrete purlins with and without CFRP strengthening," *Construction and Building Materials*, vol. 275, Article ID 122173, 2021.

[23] M. H. Arslan, Ş. Yazman, A. A. Hamad, C. Aksoylu, Y. O. Özkılıç, and L. Gemi, "Shear strengthening of reinforced concrete T-beams with anchored and non-anchored CFRP fabrics," *Structures*, vol. 39, pp. 527–542, 2022.

[24] L. Gemi, M. Alsdudi, C. Aksoylu, Ş. Yazman, and Y. O. Özk, "Optimum amount of CFRP for strengthening shear deficient reinforced concrete beams," *Steel and Composite Structures*, vol. 43, no. 6, pp. 735–757, 2022.

[25] Y. O. Özkılıç, L. Gemi, E. Madenci, and C. Aksoylu, "Effects of stirrup spacing on shear performance of hybrid composite beams produced by pultruded GFRP profile infilled with reinforced concrete," *Archives of Civil and Mechanical Engineering*, vol. 23, Article ID 36, 2023.

[26] E. Aydın, E. Boru, and F. Aydın, "Effects of FRP bar type and fiber reinforced concrete on the flexural behavior of hybrid beams," *Construction and Building Materials*, vol. 279, Article ID 122407, 2021.

[27] A. Saribiyik, B. Abodan, and M. T. Balci, "Experimental study on shear strengthening of RC beams with basalt FRP strips

using different wrapping methods," *Engineering Science and Technology, an International Journal*, vol. 24, no. 1, pp. 192–204, 2021.

[28] S. K. Kamane, N. K. Patil, and B. R. Patagundi, "Prediction of twisting performance of steel I beam bonded exteriorly with fiber reinforced polymer sheet by using neural network," *Materials Today: Proceedings*, vol. 43, Part 1, pp. 514–519, 2021.

[29] E. Aydin and M. Aktas, "Obtaining a permanent repair by using GFRP in steel plates reformed by heat-treatment," *Thin-Walled Structures*, vol. 94, pp. 13–22, 2015.

[30] S. Kumaraguru and P. Alagusundaramoorthy, "Flexural strengthening of steel beams using pultruded CFRP composite sheets with anchorage mechanisms," *Structures*, vol. 33, pp. 1414–1427, 2021.

[31] E. Ghafoori and M. Motavalli, "Normal, high and ultra-high modulus carbon fiber-reinforced polymer laminates for bonded and un-bonded strengthening of steel beams," *Materials & Design*, vol. 67, pp. 232–243, 2015.

[32] V. H. Jariwala, P. V. Patel, and S. P. Purohit, "Strengthening of RC beams subjected to combined torsion and bending with GFRP composites," *Procedia Engineering*, vol. 51, pp. 282–289, 2013.

[33] A. Hadhood, M. G. Gouda, M. H. Agamy, H. M. Mohamed, and A. Sherif, "Torsion in concrete beams reinforced with GFRP spirals," *Engineering Structures*, vol. 206, Article ID 110174, 2020.

[34] Q. L. Wang, M. Chu, and K. Peng, "Study on torsional performance of square concrete filled CFRP-steel tubes," *Arabian Journal for Science and Engineering*, vol. 47, pp. 13499–13522, 2022.

[35] P. Kuan, W. Qing-Li, and S. Yong-Bo, "Experimental study on torsional behaviour of square concrete filled CFRP-steel tube (S-CF-CFRP-ST)," *Journal of Constructional Steel Research*, vol. 193, Article ID 107295, 2022.

[36] ASTM A370-10, *Standard Test Methods and Definitions for Mechanical Testing of Steel Products*, ASTM (American Society for Testing and Materials), 2010.

[37] F. P. Beer and E. R. Johnston, *Cisimlerin Mukavemeti*, Beta Publisher, Türkiye, 1st edition, 2003.

[38] Version 6.13. Abaqus Analysis User's Manual, *Abaqus Analysis user's Manual*, ABAQUS, Inc, Providence, RI, 2013.

[39] Y. Dai, K. Roy, Z. Fang, B. Chen, G. M. Raftery, and J. B. P. Lim, "A novel machine learning model to predict the moment capacity of cold-formed steel channel beams with edge-stiffened and un-stiffened web holes," *Journal of Building Engineering*, vol. 53, Article ID 104592, 2022.

[40] Z. Fang, K. Roy, Y. Dai, and J. B. P. Lim, "Effect of web perforations on end-two-flange web crippling behaviour of roll-formed aluminium alloy unlipped channels through experimental test, numerical simulation and deep learning," *Thin-Walled Structures*, vol. 179, Article ID 109489, 2022.

[41] B. Chen, K. Roy, A. Uzzaman, and J. B. P. Lim, "Moment capacity of cold-formed channel beams with edge-stiffened web holes, un-stiffened web holes and plain webs," *Thin-Walled Structures*, vol. 157, Article ID 107070, 2020.

[42] Z. Fang, K. Roy, J. Xu, Y. Dai, B. Paul, and J. B. P. Lim, "A novel machine learning method to investigate the web crippling behaviour of perforated roll-formed aluminium alloy unlipped channels under interior-two flange loading," *Journal of Building Engineering*, vol. 51, Article ID 104261, 2022.

[43] Y. Dai, K. Roy, Z. Fang, G. M. Raftery, and J. B. P. Lim, "Structural performance of cold-formed steel face-to-face built-up channel sections under axial compression at high temperatures through finite element modelling," *Buildings*, vol. 13, no. 2, Article ID 305, 2023.